Virtual Touch:

Tagging ultrasound-based Haptics

Radovan Vodila^a and Klaas Bombeke^b

 a University of Innsbruck ^bDepartment of Communication Sciences, imec-mict-UGent, Ghent University

Word Count: 5620

Author Note

Correspondence concerning this article should be addressed to Radovan Vodila:

radovodila@gmail.com

Abstract

Touchless interfaces represent a promising advancement in human-machine interaction, with midair haptic interfaces gaining significant attention. These interfaces use focal ultrasound (US) beams projected onto the skin to create vibrational sensations, enabling dynamic haptic feedback through hand tracking. This technology has broad applications across industries such as automotive, extended reality, medical training, and immersive marketing.

To the best of our knowledge, this EEG study is first to extend frequency-tagged neural markers to the domain of ultrasound-based haptics. Specifically, a low-frequency haptic pulse was employed to drive steady-state somatosensory evoked potentials (SSSEPs) in subjects EEG, which was then analyzed by spectral analysis and multivariate generalized eigendecomposition (GED).

EEG analysis results indicate substantial difficulties in entraining the frequency tag, as no distinct peak in the driving frequency was found in sensor-space. Moreover, power spectral density (PSD) analysis reveals a suppression in the driving frequency both in absolute values and partly also relative to ipsilateral sites for some cases. GED analysis however, points towards an entrainment of the driving frequency in accordance with the somatosensory template. Additionally, highly variable results between and within participants were observed in terms of PSD estimations and GED components, which are discussed in the limitations section.

Despite the inconclusive results, this pilot study provides valuable insights for informing a refined experimental protocol for large-scale execution on establishing reliable neural markers for ultrasound-based haptics. This conceptual foundation can be used to generate comparability with traditional haptics on a neural level, making way for investigations of cognitive processes such as attentive biases in operator systems.

Introduction

Touchless haptic interfaces, such as those produced by Ultraleap, represent a significant advancement in human-computer interaction technology. These interfaces allow users to experience tactile sensations and control devices without physical contact. Leveraging ultrasound technology, touchless haptic interfaces create a more immersive and hygienic (imec, 2020) user experience across various applications, from virtual reality to automotive industry (Large, Harrington, Burnett, & Georgiou, 2019). In automotive applications, integrating ultrasound-based haptics into gesture control systems offers significant advantages. For example, Bosch and Harman Group are developing systems that allow drivers to control various in-vehicle functions through hand gestures detected by devices like the LEAP Motion Controller. (Ultraleap, 2019). The company argues that this setup minimizes the need for drivers to look at or touch physical controls, reducing visual demand and potential distractions. (Shakeri, Williamson & Brewster, 2018). Focused ultrasound provides precise tactile feedback, improving usability and safety. Another promising application is to use haptic feedback as an alert signal. Picture a vehicle driving in autonomous mode. Suddenly, the conditions change, and the driver needs to be prompted to take back control of the machine. A haptic alert can augment the traditional modes of interaction, such as visual and auditory.

The evolution towards touchless haptics was driven by the need for more intuitive and natural user interfaces. In the 2000s, research into the use of ultrasound to create tactile sensations in mid-air gained momentum.[(Hoshi, Iwamoto, & Shinoda, 2009), (Hoshi, Takahashi, Iwamoto, & Shinoda, 2010), see (Chouvardas, Miliou, & Hatalis, 2008) for review]. This led to the founding of Ultrahaptics, now rebranded to Ultraleap, in 2013 as a spin-off of the University of Bristol.

Touchless haptic interfaces utilize ultrasound waves to create tactile sensations on the user's skin. The technology involves an array of ultrasonic transducers that emit high-frequency sound waves. These waves converge to form precise points of acoustic radiation pressure, which can be felt as tactile sensations by the user. Acoustic pressure is interpreted by the same sensors – called mechanoreceptors - that detect tactile sensations. Mechanoreceptors in the human skin, such as Meissner corpuscles and Pacinian corpuscles, respond optimally to specific frequency ranges. Meissner corpuscles are sensitive to light touch and low-frequency vibrations around 30-50 Hz, while Pacinian corpuscles detect higher-frequency vibrations in the range of 250-350 Hz. These

mechanoreceptors work by converting mechanical stimuli into electrical signals that are transmitted to the brain, allowing us to perceive touch and vibration. (Abraira & Ginty, 2013). Ultrasound-based haptics can precisely target these receptors by emitting sound waves at their optimal frequencies, thereby creating realistic and detailed tactile feedback without the need for physical contact.

By modulating the amplitude and phase of the ultrasound waves, the system can create various textures and sensations, simulating the feel of buttons, sliders, and other interactive elements. (Carter, Seah, Long, Drinkwater, & Subramanian, 2013).

A key component of Ultraleap's system is the Leap Motion Controller, which tracks hand movements with high precision using infrared sensors. This data is then used to adjust the ultrasound waves in real time, ensuring that the tactile feedback corresponds accurately to the user's hand position and movements. This integration of hand tracking and haptic feedback enables users to interact with virtual objects as if they were physically present.

Haptic interfaces in operator systems are widely adapted in commercial and industrial applications. The most common mode of haptic interface is the vibrotactile one: Utilizing small actuators that produce vibrations, most commonly based on rotary or piezo-based architectures. Piezo-based haptic actuators produce precise and rapid tactile feedback by converting electrical energy into mechanical motion. (see Song et al., 2023 for review). Pneumatic haptic interfaces use air pressure to create tactile sensations by inflating and deflating small air bladders. Pneumatic systems are effective in simulating realistic textures and are commonly used in medical training simulators for replicating the feel of human tissues. (See Sénac et al., 2019).

Ultrasound-based haptics distinguish themselves from pneumatic and vibrotactile haptics by providing contactless tactile feedback, essentially decoupling haptic sensations from physical surfaces and offering significant advantages in hygiene, versatility, and user experience. As this technology evolves, integrating neural markers becomes crucial to optimizing and validating these haptic systems, ensuring that the tactile feedback aligns seamlessly with the user's cognitive and neural responses, thereby enhancing the intuitiveness and effectiveness of the interactions.

Establishing Neural Markers for Touchless Haptic Technology

To fully understand and optimize touchless haptic interfaces, it is best practice to establish neural markers that reflect the brain's response to these stimuli. Frequency tagging is a method employed in the cognitive neurosciences, which involves the presentation of periodic stimuli at specific frequencies to evoke steady-state evoked potentials (SSEPs) in M/EEG. [(Nozaradan, 2014), (Wieser, Miskovic, & Keil, 2016)]. Frequency tagging relies on rhythmic sensory stimulation that can be observed in the spectral domain of the EEG signal. Stimulation thus does not need to be time-locked to specific experimental events or produce temporal markers against which the EEG signal can be investigated. This is convenient, since we could not reliably link the ultrasound stimulation system with the EEG system to yield precise temporal markers of stimulation.

Frequency Tagging and Steady-State Evoked Potentials (SSEPs)

Frequency tagging leverages the phenomenon that a sensory stimulus modulated at a specific frequency leads to neural oscillations, which map onto the stimulation frequency. When a stimulus is presented at a constant frequency, a neural oscillation of the same frequency is entrained in the brain. This phenomenon holds true in the visual (Norcia, Appelbaum, Ales, Cottereau, & Rossion, 2015), auditory [(Drijvers, Jensen, & Spaak, 2021), (Vos, Collignon, & Boets, 2023)], somatosensory [(Brickwedde, Schmidt, Krüger, & Dinse, 2020), (Breitwieser, Kaiser, Neuper, & Müller-Putz, 2012)] and nociceptive domain (Colon, Legrain, & Mouraux, 2012).

This entrained activity is then called SSEPs and can be found in the spectral analysis of the M/EEG signal. For example, a 24 Hz visual flicker stimulus entrains a 24 Hz oscillation in the visual cortex. A 13 Hz modulated tone entrains a 13 Hz oscillation in the primary auditory cortex. Notably, the power of the entrained frequency component depends on the asserted attention and the natural tuning to the frequency. For somatosensory stimuli, Tobimatsu et al. (2019) have found 21 Hz to be the optimal frequency for maximizing the amplitude of steady-state somatosensory evoked potentials (SSSEPs).

This pilot aims to test whether this technique can be extended to the ultrasound-based haptic domain. To apply frequency tagging to touchless haptic interfaces, the plan was to project flickers of haptic touch onto the palm of the hand and see whether SSSEPs

manifest in the somatosensory cortex. This way, one wouldn't have to worry about a lack of synchronization of the EEG system with the Stratos array, as the oscillations manifest after approximately 500 milliseconds and remain stable while the flicker continues. (Brickwedde et al., 2020). With this consideration in mind, a rough time-lock of stimulus onset would suffice for a frequency decomposition of the following period of 20 seconds.

Analyzing the entrained SSEPs will provide insights into how the brain perceives and processes touchless haptic feedback, informing the optimization of these interfaces for various applications. Establishing these neural markers is essential for advancing the development of touchless haptic technology, ensuring that it not only mimics physical touch effectively but also integrates seamlessly with human sensory processing systems.

In summary, this pilot was conducted to test whether somatosensory SSEPs can be used as neural markers for Ultrasound-based haptic stimulation. To test for manifested SSEPs, an US-based flicker stimulus was projected onto participants hands - Taking the contralateral processing of somatosensory stimulation into account, we expected to retrieve the tag on sites contralateral to the stimulated hand in the centroparietal sensors lateral to the midline. (Hari et al., 1990). The relative power distribution of this band was expected to differ significantly between participants and conditions due to idiosyncratic variance in perceiving the stimulus across the experiment. However, a peak in 3Hz is expected across conditions and participants. In GED, component maps with strong weighting in the respective region of interest (ROI) are expected.

Methods

Materials

The study utilized the Ultrahaptics Development Kit 1 (UHDK1) by Ultraleap, specifically designed for touchless haptic feedback. This system employs focused ultrasound (US) beams to create tactile sensations in midair, allowing users to feel virtual objects and textures without physical contact. The UHDK1 includes the Stratos haptic array, a sophisticated device that projects highly focused ultrasound beams onto the user's skin. The array is capable of generating a wide range of tactile sensations, including simple shapes like triangles and spheres by precisely controlling the ultrasound beam's focus and movement. Additionally, the system incorporates a hand tracker, which enables the device to map the haptic sensations onto the user's hand and follow its movements. This feature makes the haptic feedback non-stationary, dynamic, and adaptable to the user's

movements, enhancing the realism and responsiveness of the virtual touch experience. Ultraleap's Stratos platform utilizes ultrasonic transducers operating at 40 kHz to create mid-air haptic sensations. This carrier frequency is modulated by a 200 Hz signal, which affords interpretability by human mechanoreceptors. The transducers emit focused sound waves that converge to form tactile feedback, which can be felt by the user's hands without physical contact. The technology leverages the patented Time Point Streaming (TPS) to enable high-refresh-rate and complex haptic feedback, allowing for detailed rendering of 3D shapes and textures. In total, the UHDK1 array featured 256 transducers. (Ultraleap, n.d.).

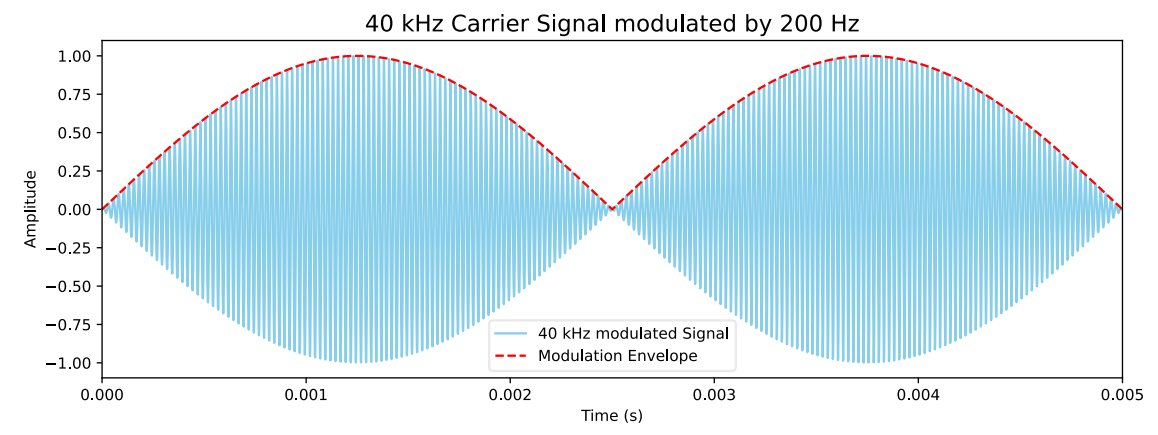


Fig. 1: A schematic of a 40 kHz ultrasound pressure wave (blue) by a 200 Hz modulation signal (red) to create perceivable mid-air tactile sensations.

For EEG data acquisition, the ANTNeuro eego™mylab system with a 64-channel configuration and 1024 Hz sampling rate was employed. (ANTNeuro, n.d.). Additionally, an EOG sensor was integrated in the acquisition, making the total number of active sensors 65. Electrodes were positioned according to the international 10-20 system. The eego amplifier is actively shielded to minimize 50 Hz line noise.

Participants

Nine subjects participated in this pilot study, but six data sets were discarded due to flawed acquisition and changes in the experimental design, leaving three data sets suitable for analysis (n = 3). Participants sat with their hands comfortably placed on a custom handrest with a cut-out designed to allow the ultrasound waves to reach their hands unhindered. They were instructed to adjust their hand position to maximize the subjective sensory sensation, and this calibration was repeated after switching hands.

Procedure

The main body of the experimental design consisted of four conditions with five 40-second trials each. The ultrasound flicker was successively directed to the palm and fingers of both the left and right hand. Each trial comprised two 20-second periods, with a 2 Hz flicker followed by a 3 Hz flicker. The only variable within a trial was the flicker frequency. To keep participants attentive, they were instructed to lift a finger of the contralateral hand upon sensing a change in frequency. Additionally, a 60-second baseline period was recorded before the flicker trains. Lastly, Participants were asked which hand placement resulted in the strongest sensations and the preferred location was used for 60-second continuous stimulation.

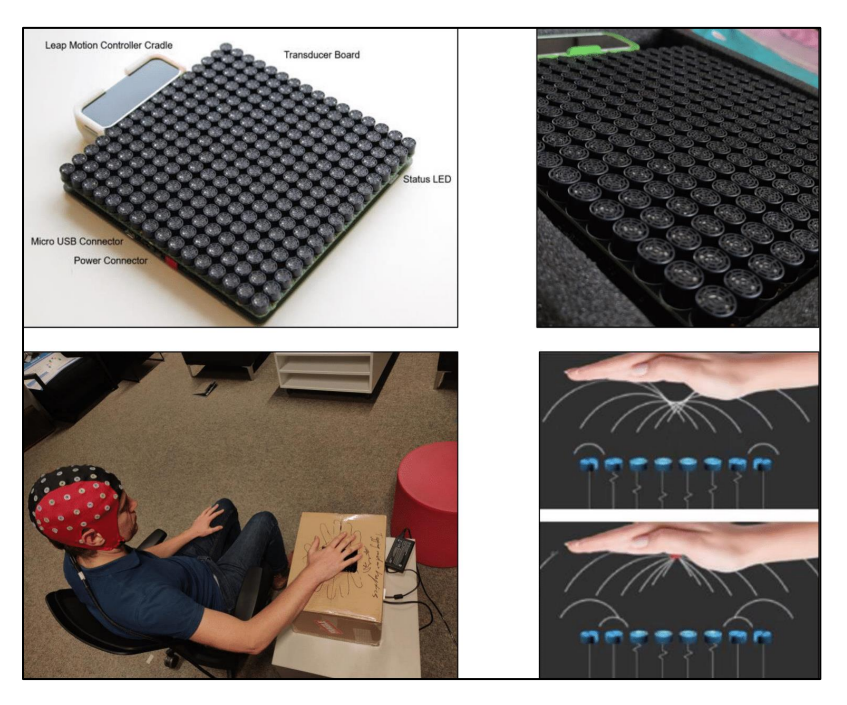


Fig. 2: Upper left: UltraHaptics Development Kit 1 (UHDK1) with an integrated Leapmotion handtracker of the same firm*. Upper right: Transducer-close-up of the device as used in the study. Lower left: A snapshot of the experiment being conducted. Note the gap between hand and the cut-out of the box. Lower right: Haptic air pressure is generated by constructive interference of mechanical waves forming focal points in the air*

Preprocessing

Raw time-series was inspected visually. Then, data was filtered off-line between 1 and 40 Hz using a Butterworth band-pass filter. Electrical distance between electrodes was computed to scan for bridged electrodes. Electrode bridging occurs when two or more electrodes in an electrophysiological recording system are electrically connected, usually due to the presence of a conductive substance like sweat or gel spillover. Bridged channels

carry highly correlated signal and can introduce artefacts and distort the recorded signals. Therefore, bridged electrode clusters were excluded in a way, such that only one electrode of a bridged cluster remained. ICA, a computational method used to separate a multivariate signal into additive and independent components, yielded no troubling artefactual components and thus all were retained. This method is commonly used for artefact rejection such as eye- or muscle-based activity. In this case, participants were instructed to keep their eyes closed and not to move, so components matching the eye template were only sparsely distributed.

The preprocessed data was epoched into 40-second trials, each consisting of two 20-second periods. Subsequently, half of the electrodes were removed, excluding the frontopolar, frontal, parieto-occipital, and occipital electrodes. This reduction in electrode count aimed to result in cleaner components. Such sparsity approach has proven effective in minimizing noise in previous work. (Rosso, 2023).

Analysis

Analysis was run on Python 3.12.4 utilizing the libraries matplotlib, MNE, NumPy, pickle, and SciPy. Data was analyzed by a channel-wise PSD computation and generalized eigendecomposition (see Cohen, 2022. & Cohen, 2021) using the MNE library in Python (Gramfort et al., 2013), along with NumPy (Harris et al., 2020) and SciPy (Virtanen et al., 2020).

For univariate analysis in frequency space, Power Spectral Density (PSD) estimation was conducted to analyze periodicities and identify dominant frequencies in time-series data. The Fast Fourier Transform (FFT) was then used for spectral decomposition. Epochs were trimmed to only include the 3 Hz stimulation period for ease of visualization. The extracted PSD values of palm and finger stimulation trials from each hand were aggregated per participant. Six channels were identified as the region of interest (ROI) per side, located posterior and lateral to the vertex, thus covering the second sensorimotor cortex. (Left ROI: CP1, CP3, CP5, C1, C3, C5, and right ROI: CP2, CP4, CP6, C2, C4, C6).

Odd-numbered electrodes were on the left hemisphere, and even-numbered electrodes were on the right. Thus, the left condition featured right-sided (even) electrodes and viceversa. Additionally, condition-wise power differences between left and right regions of interest (ROIs) were inspected. For each condition, the channel-resolved PSDs of the expected (contralateral) ROI were contrasted against the ipsilateral one. Electrodes were

paired, and their power was point-wise subtracted to highlight the relative differences in brain activity between the two ROIs.

As the second axis of analysis, generalized eigendecomposition (GED) was conducted. This involves solving the generalized eigenvalue problem defined by the equation

$$Sw = \lambda Rw$$

where S is the covariance matrix of the signal of interest, and R is the covariance matrix of the reference signal. The eigenvector w (spatial filter) associated with the eigenvalue λ is sought to maximize the variance of the signal of interest while minimizing the variance of the reference signal. If the data are organized in a channels-by-time matrix X, then the covariance matrix for the signal of interest, S, can be computed as $S = X_s X_s^T$, where X_s is the signal matrix. Similarly, the covariance matrix for the reference signal, R, is given by $R = X_r X_r^T$, where X_r is the reference signal matrix.

The goal of GED in this context is to derive a spatial filter \mathbf{w} that optimally enhances the contrast between the signal of interest and the reference signal. This spatial filter is represented by the eigenvector corresponding to the largest eigenvalue, λ which quantifies the ratio of the variances of the signal of interest to the reference signal. GED is an advanced algorithm similar to principal component analysis (PCA) but is informed by the trial design and not bound by the orthogonality assumption of components. Unlike PCA, which is a blind source separation technique that does not take experimental conditions into account, GED returns a spatial filter of electrode weights that maximize a pre-specified contrast, such as differences in spectral power between conditions. By decomposing covariance matrices from a stimulus and reference condition, GED identifies spatial filters that maximize the variance between different experimental conditions while minimizing within-condition variance. This method exploits the contrast defined in the trial design. Within one trial, two periods of stimulation occur, differing only in one attribute: the flicker frequency. The thereby entrained steady-state evoked potentials (SSEPs) define the contrast for this method.

For this, a subset of 30 channels was selected. GED relies fully on the quality of the **S** and **R** matrix whose product is diagonalized by GED. The pipeline of computation is as follows: Trials were cropped to only feature the 3 Hz stimulation (18 seconds). Per subject and per condition, all trials were stitched into an array. For **S**, the time series was band-pass filtered between 2.5 and 3.5 Hz. For **R**, the data was kept in broad-band.

The procedure from this point on is identical for both arrays. The array was segmented into 2-second parcels, and for each parcel, a channel-by-channel covariance matrix was computed. All matrices were then averaged to create the S and R matrix for the subsequent GED. In total, * subjects * 4 condition * 2 = 24 covariance matrices.

The resulting eigenvalues from this decomposition are then sorted in descending order and normalized against the strongest eigenvalue to form a power ratio. To visualize the variance explained by each eigenvalue, a scree plot is created, plotting the normalized eigenvalues against their respective ranks.

Choosing the averaging approach for computing covariance matrices allows for capturing the temporal dynamics of the EEG signal, which could be lost with a single, global covariance matrix. Additionally, averaging covariance matrices from smaller chunks can reveal subtle, time-specific relationships between channels that a whole-series approach might obscure. This method enhances the sensitivity of GED to detect variations in spectral power and other neural dynamics, ensuring that transient and periodic phenomena are accurately represented in the analysis. Importantly, this segmented approach introduces a nonlinear operation that can capture complex interactions and nonlinear dependencies in the EEG data, which might not be evident through linear methods alone. All processing steps were identical for the participants. Code and data files can be found on the corresponding Github repository.

Results

This study employed generalized eigenvalue decomposition (GED) analysis on EEG data (n = 3) to trace somatosensory steady-state evoked potentials under four different conditions of ultrasound-based flicker stimulation: right palm, left palm, left fingers, and right fingers. The aim was to observe the brain's thereby entrained responses and compare the spatial and spectral characteristics of the GED components across these conditions and participants.

Univariate Analysis

Figure 3 shows the averaged Power Spectral Density (PSD) plots for six channels for three participants under left and right conditions. The main focus is on the 3 Hz stimulation frequency and its surrounding frequencies to analyze the neural response to the 3 Hz stimulation. No 3 Hz peak is visible across participants in the provided PSD plots,

indicating a lack of clear entrainment to the stimulation frequency. Contrary to expectations, subjects 0 and 5 even show a suppression in the driving frequency in the left condition. This is peculiar, as it contradicts the hypothesis and workings of SSEPs. Only subject 1 in the left stimulation conditions shows a slight peak in the driving frequency. In short, there is no indication of successful entrainment across the participants from spectral analysis of sensors.

Figure 4 illustrates the channel-resolved power differences between left and right ROI for each condition. To aggregate left and right hemisphere differences, electrodes were paired, and their power values subtracted. Positive values read as more power in the expected ROI, and negative values read as more power in the ipsilateral sites. Subject 0 depicts hypothesis-coherent power differences for right conditions, but curiously enough, this trend is reversed for left conditions. Precisely at 3 Hz, ROI sensors for left conditions show weaker power than ipsilateral sites. It is important to note that the two conditions depict relative relations and are not based on the same data. The patterns in subject 0 indicate that in both left and right stimulation, entrainment in the right hemisphere was dominant relative to the left ROI sensors. Both subject 1 and subject 5 show noisy data around 3 Hz with a peak in right conditions at 3.3 Hz driven by C6/CP6 sensors. subject 5 also shows a peak in CP5 close to the driving frequency. The positive deflections indicate that there was higher power in the contralateral sites as opposed to the ipsilateral ones.

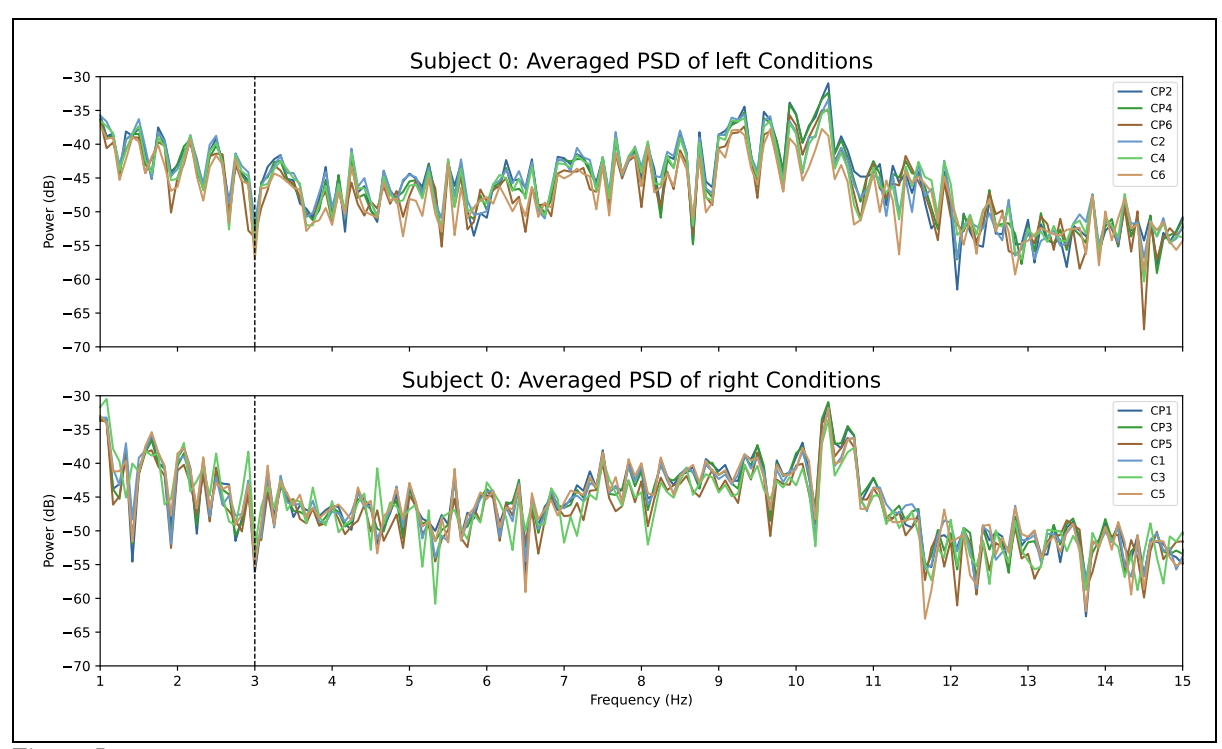


Fig. 3 – I.

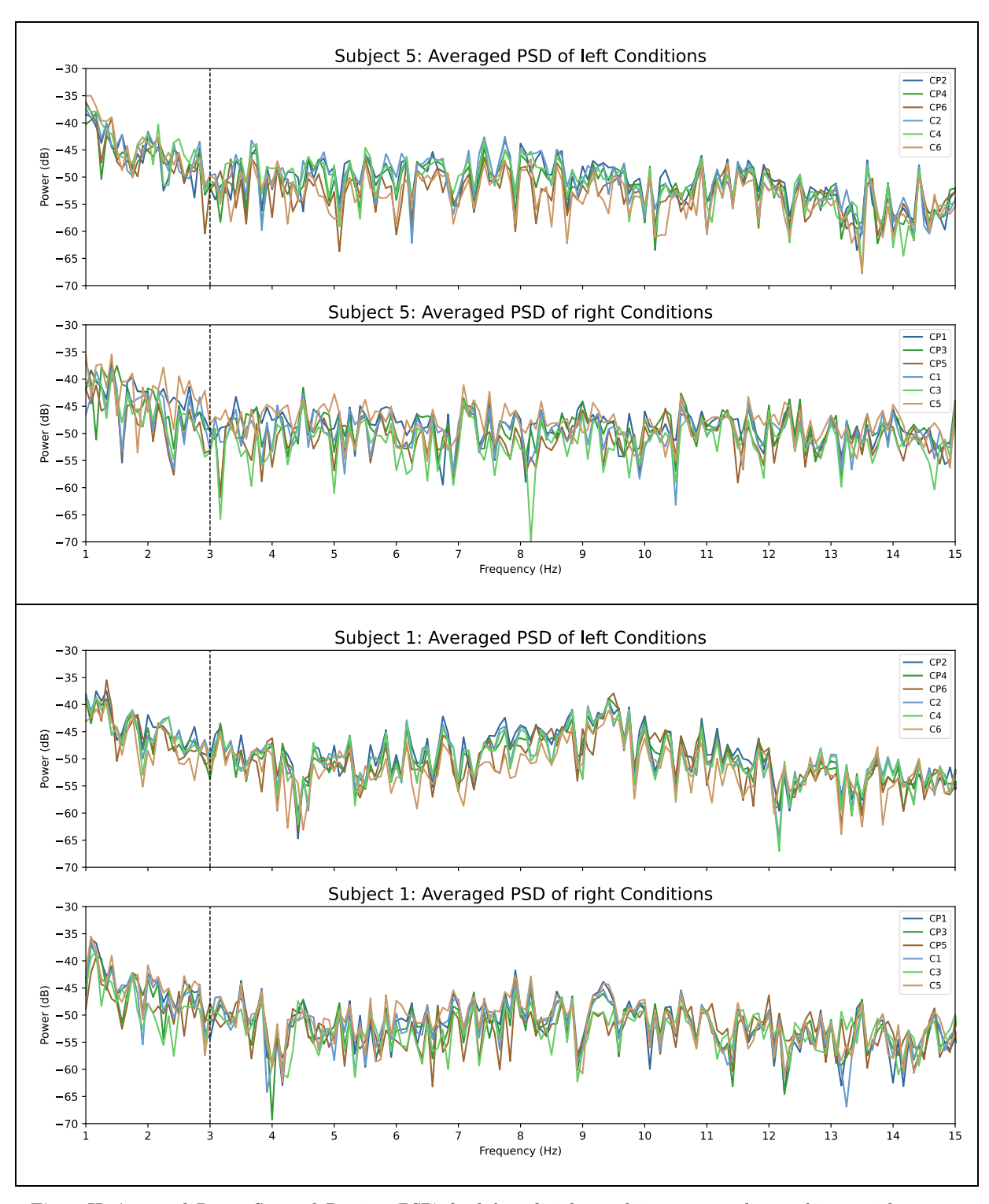


Fig. 3-II: Averaged Power Spectral Density (PSD) for left and right conditions across three subjects, with power measured in decibels (dB) on a logarithmic scale. The color codes position along the midline. Lighter shades indicate posterior electrodes whereas darker shades represent electrodes on the vertex. The same color code is applied to both sides.

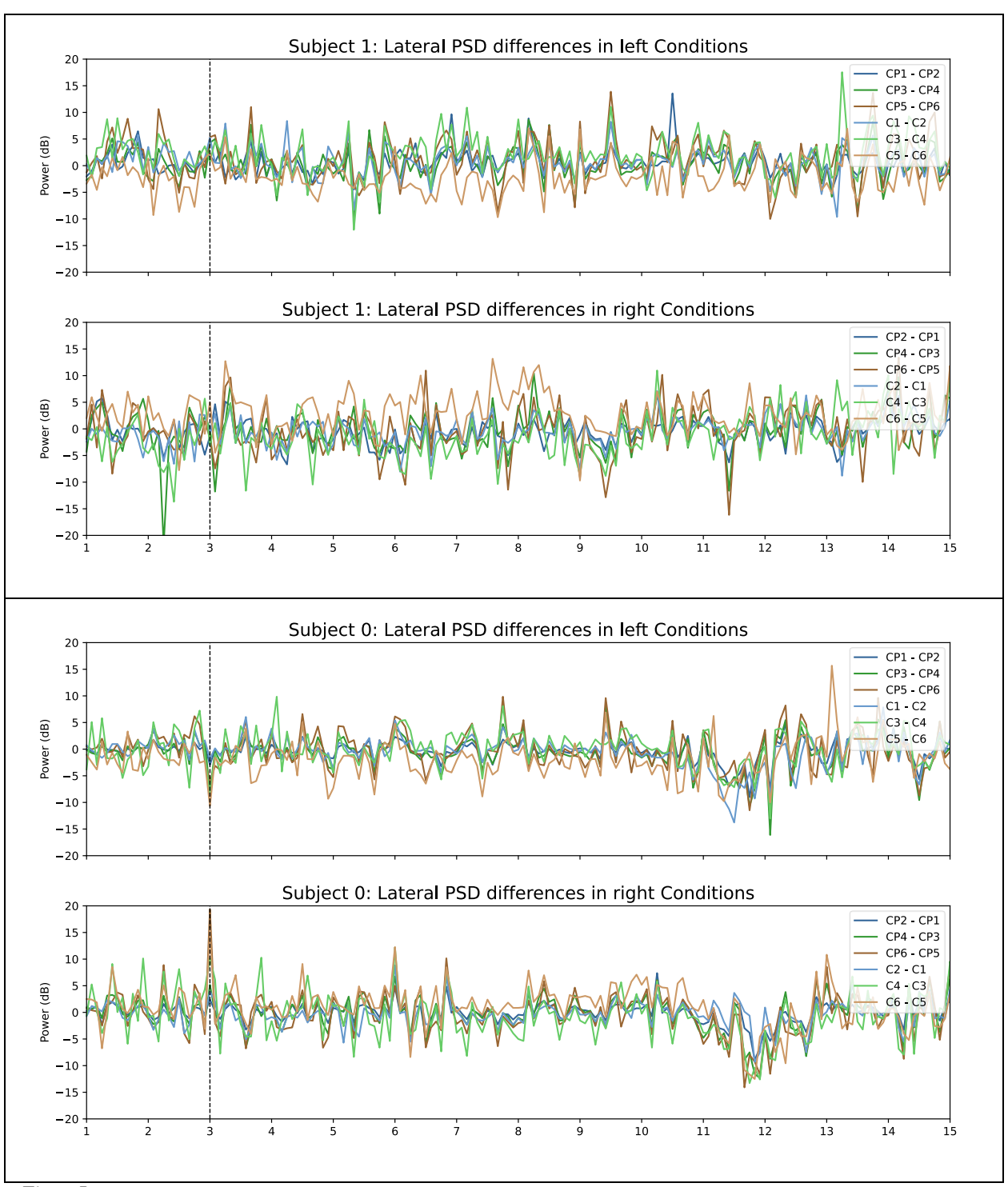


Fig. 4-I.

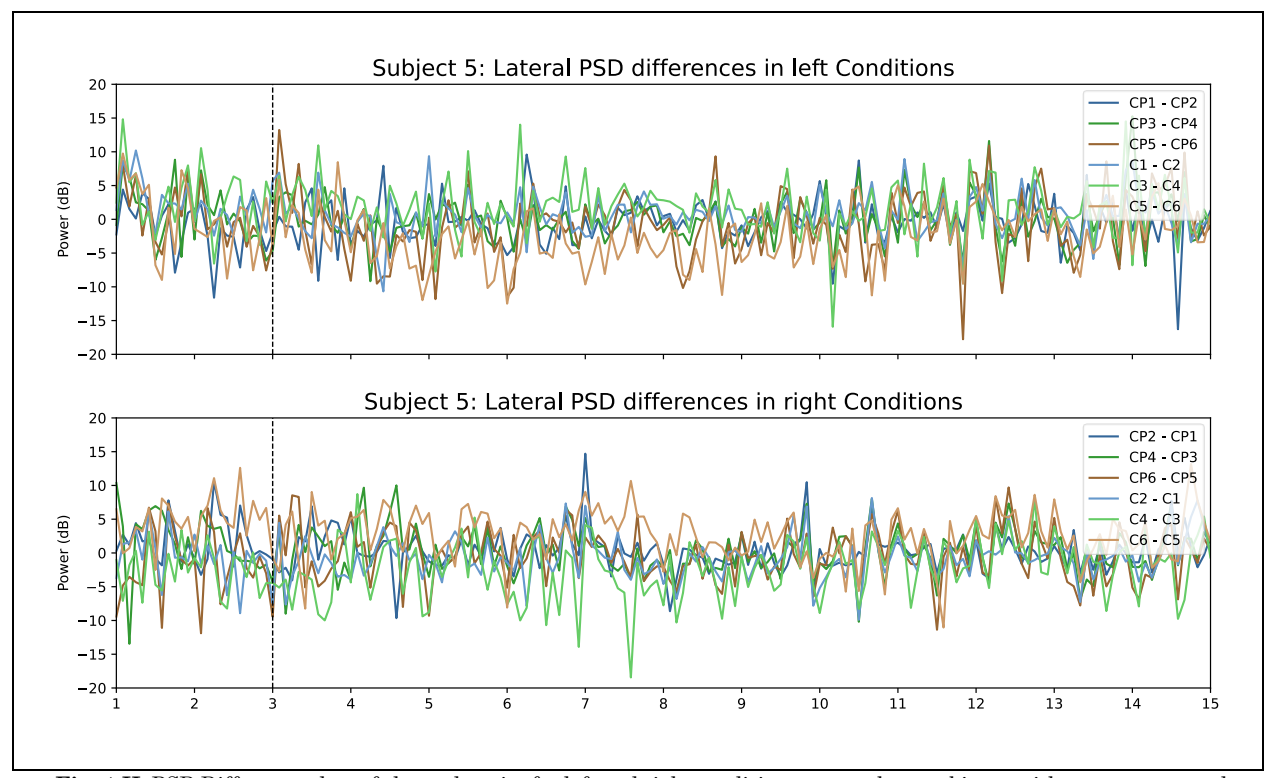


Fig. 4-II: PSD Difference plots of electrode pairs for left and right conditions across three subjects, with power measured in decibels (dB) on a logarithmic scale. The PSD of ipsilateral sensors were subtracted from sensors of the contralateral region of interest. Positive values indicate more power in the contralateral region, whereas negative values point to lower power. The color codes position along the midline. Lighter shades indicate posterior electrodes whereas darker shades represent electrodes on the vertex. The same color code is applied to both sides

Multivariate Analysis

It's expected that conditions involving stimulation on the left side evoke activity on the right around electrode CP3 and CP4, respectively as these on top of the somatosensory cortex. Importantly, the components spectral features extracted with GED are not narrow band. Although one expects a prominence of the target frequency (because electrodes featuring that spectral content are weighted more), it is still expected to have background broadband activity - including the individual 1/f curve .WHERE.curve. The 1/f power distribution, also known as pink noise, describes a signal whose power spectral density is inversely proportional to its frequency, indicating more power at lower frequencies and less at higher frequencies. (see Wen & Liu, 2016 for review).

Results reveal substantial variability both within and between participants. Each of the following figures presents the spatial weights of the first GED component and its corresponding PSD plot. The PSD was calculated by applying the component weights to the time series used in the covariance matrix and then performing spectral decomposition. The spectral peaks in the band of interest (2.5 - 3.5 Hz) remain stable across conditions

but differ substantially between subjects 0 and 1 by 0.74 Hz, despite both being stimulated at 3 Hz.

For participant 0, the expected contralateral activation was observed in three out of four conditions. The exception was the "right fingers" condition, which is characterized by an obscure spatial pattern. The PSD plots for participant 0 consistently show a prominent spectral peak at 2.37 Hz, indicating the frequency at which the maximum power is observed. Additionally, an unexpected peak at 0.47 Hz was noted, which is the fifth subharmonic of the maximum frequency. This subharmonic presence might point to an unusual frequency response not observed in the other participants.

By contrast, participant 1 displayed the expected contralateral activation only in the "left fingers" condition. Interestingly, the "right fingers" condition exhibited ipsilateral SSEP entrainment, where the brain activity occurred on the same side as the stimulation. The PSD plots for participant 1 revealed a spectral peak at 3.11 Hz, aligning with the 3 Hz stimulation frequency. Participant 5 did not exhibit any notable spectral peaks across its conditions. This is peculiar, as the PSD is computed from the component-weighted time series, which is informed to maximize between-matrix variance and thus maximize the contrast of 3 Hz. The time series should be thus by definition characterized by a strong 3 Hz component. The absence of a notable peak in the PSD for participant 5 suggests that the component does not effectively capture the informed contrast - possibly due to individual differences in neural processing or issues related to data quality.

Eigenspectrum Scree plots display the eigenvalues of components in descending order, showing how much variance each component captures - normalized against the strongest eigenvalue.

Participant 0 exhibits scree plots with a clear decreasing trend. The first few components capture the most variance, followed by a steep decline - the typical pattern of variance distribution. Half of subject 1's scree plots also demonstrate the expected decreasing trend, similar to participant 0. Two conditions of subj. 1 however and all of subj. 5 however, output a flat spectrum. indicating that the power ratio (λ) is consistent across all components. This flatness is peculiar as it suggests that no single component explains significantly more variance than the others. This pattern can arise due to several factors, including homogeneous data where no distinct patterns or features dominate, or data that is heavily contaminated with noise, which masks any underlying structure.

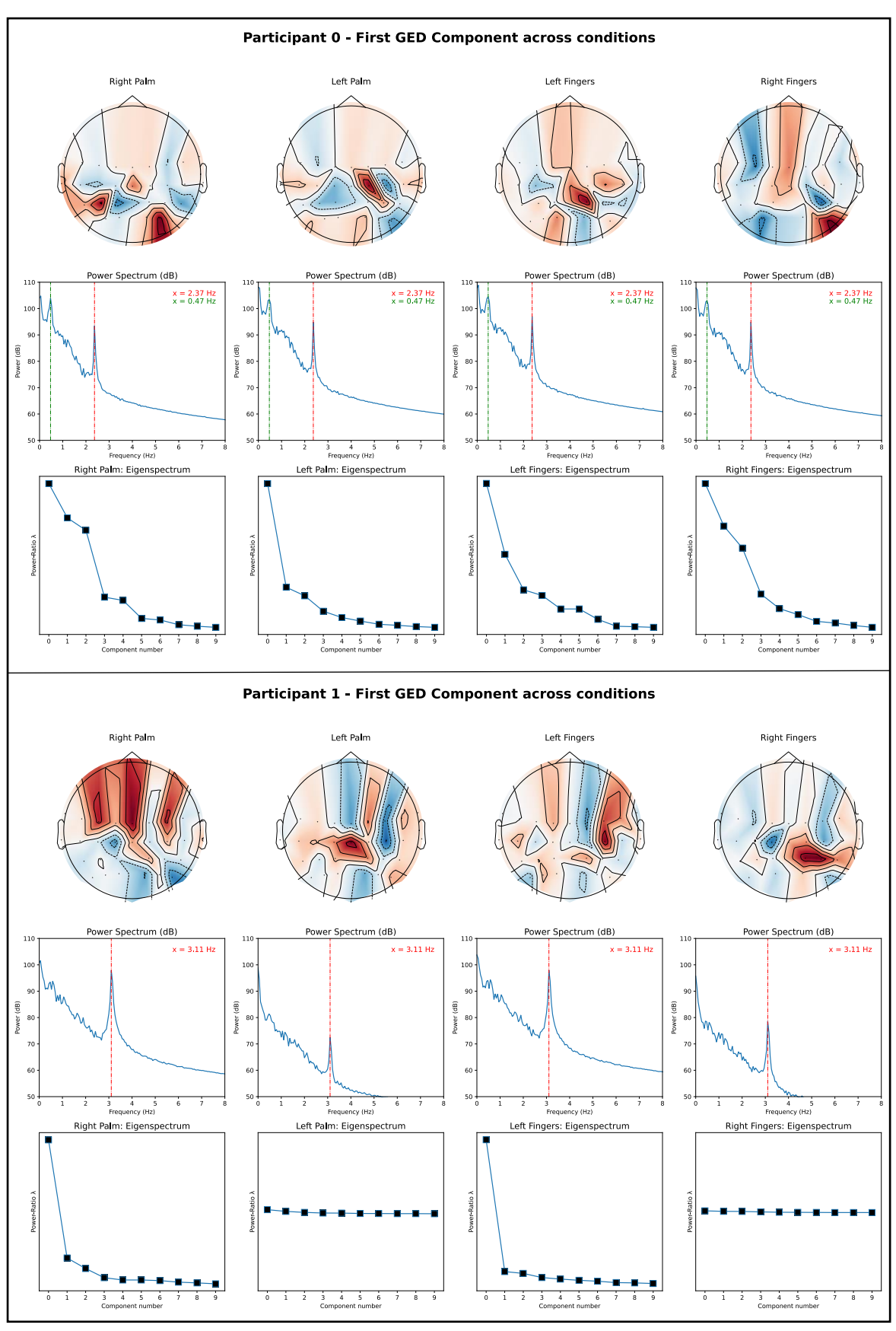


Fig. 5-I.

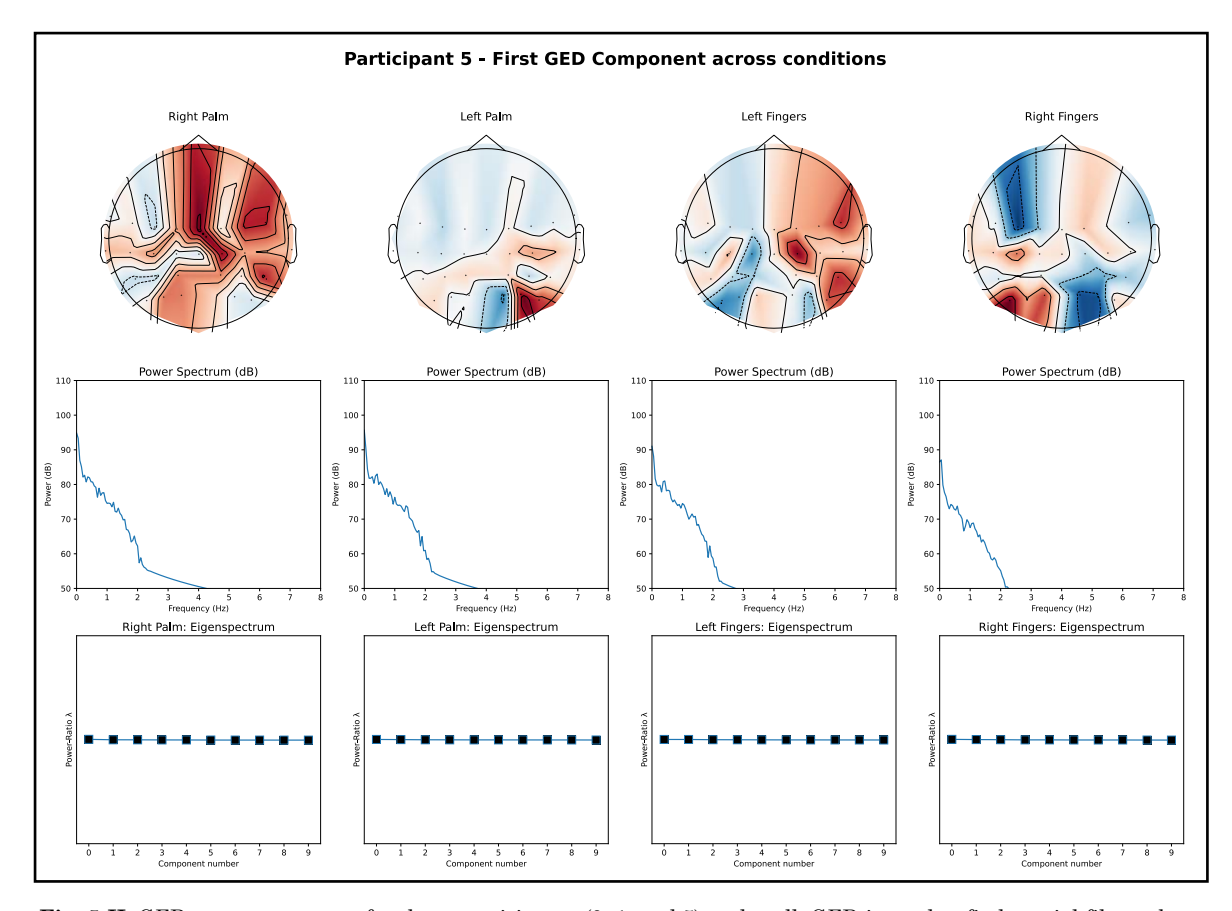


Fig. 5-II: GED component maps for three participants (0, 1, and 5) under all. GED is used to find spatial filters that maximize the signal-to-noise ratio for specific brain activity patterns. The color coding represents sensor weights, with the eigenvector projected onto linearly interpolated MNE topoplot objects. Red areas indicate strong contributions to the component, while blue areas indicate weaker contributions. The accompanying graphs show the Power Spectrum (dB) for each condition, plotted against frequency, highlighting the distribution of power across different frequencies. The third row features Eigenspectrum-Scree plots resulting from GED of each condition. It displays the eigenvalues of components in descending order, showing how much variance each component captures - normalized against the strongest eigenvalue.

Discussion

This study employed generalized eigenvalue decomposition (GED) analysis on EEG data (n = 3) to trace somatosensory steady-state evoked potentials under four different conditions of ultrasound-based flicker stimulation: right palm, left palm, left fingers, and right fingers. The aim was to observe the brain's entrained responses and compare the spatial and spectral characteristics of the GED components across these conditions and participants.

It is first to note that all means of analysis conclude in huge variance of between and within participants. Visual inspection of the PSD plots and component maps reveals highly weighted fields bordering the frontal and posterior regions for most conditions. Notably, the artifactual weighted fields of subjects 0 and 1 in the left finger and left palm

conditions seem identically localized. Ignoring these strongly weighted regions to focus solely on the somatosensory template would be hard to defend, necessitating scrutiny of data quality and the potential influence of non-target regions.

The absence of a notable 3 Hz peak in participant 5, despite the components' PSD being computed to maximize contrast at this frequency scrutinizes data quality of this participant. This is corroborated by a flat eigenspectrum of each condition. Conditions with a descending eigenspectrum curve - such as for subject 0 - suggest that the GED analysis successfully identified components accounting for the most significant variance in the data, likely reflecting genuine neural responses. The descending eigenspectrum indicates a clear separation of eigenvalues, where a few components (eigenvectors) are associated with large eigenvalues, representing significant variance in the data, allowing for the identification of principal components reflecting dominant neural activities. Conversely, the flat eigenspectrum conditions in participant 5 and partially subject 1 point towards noise or systematic errors during data acquisition. The flat spectrum lacks this separation, indicating all components contribute similarly to the variance.

GED component maps vary significantly across conditions and participants. In some conditions, highly weighted electrodes allude to SSSEPs entrained in the second somatosensory cortex. Comparing participants' peaks in the GED components with PSD, only participant 1 exhibits a matching pattern between both modes of analysis, with a peak in power at 3.1 Hz noted in the PSD of right conditions and difference plots. Subject 0's component PSD peaks at ~2.4Hz, which is not reflected in the univariate PSD plots.

The most puzzling finding is the apparent suppression of the 3 Hz across participants, most notably observed in subject 0. PSD lateral-difference plots support fortify this pattern, as right conditions show an elevated 3Hz power in contralateral sites, whereas the left condition shows higher 3Hz in ipsilateral sites. This reversal of trend within-subject is most peculiar and opens many questions. Such suppression is not easily explained, and I can only speculate it to be attributable to idiosyncratic processing and the factors elaborated in the limitations section. Further investigation is necessary to address these anomalies and enhance the reliability of neural markers for ultrasound-based haptics.

Limitations

The study design exhibits several limitations, primarily related to maintaining the subject's focus and technical implementation. Foremost, the study's low participant count (n = 3) is important to note, as it substantially limits the interpretability of results. Further, the small sample size in addition to high variance across the data prevents meaningful aggregation.

Procedural Issues

Due to limited time and resources, the study employed an improvised setup, commonly referred to as a "wizard of Oz" approach. This required manual synchronization of event triggers, with me manually pressing the triggers on both the EEG system and the device controlling the array simultaneously. This resulted in only an approximate time-lock of the flicker onset event, potentially affecting the accuracy of the recorded data. The justification for a roll-out of the study in this state was that steady-state potentials manifest after about 400 ms and therefore should be detectable within the 20 second stimulation window. This thought however assumed stability of SSEPs across the stimulation period, which is arguably invalid, as participants reported feelings of drowsiness.

The most significant issue was the inability to control for drowsiness during data acquisition. Previous research has shown that attention significantly affects SSSEP amplitude, with reduced attention in drowsy states. Participants reported frequent drowsiness, exacerbated by the instruction to keep their eyes closed. Despite attempts to mitigate this by instructing participants to lift a finger upon flicker extinguishment, drowsiness likely introduced confounding variance between and within trials. This variance could lead to GED components not being comparable across trials, diminishing the validity of averaging components across trials.

Furthermore, the haptic flickers produced auditory noise at the same frequency, with noise levels higher in the finger conditions than the palm conditions due to better coverage of the cardboard packaging box over the device. This noise could interfere with the detection of SSSEPs.

Hardware Limitations

Flicker frequencies used for stimulation was limited to low frequencies because higher frequency settings were deemed to be unstable, missing beats, or varying in frequency despite constant parameters. This instability raises questions about the accuracy of the reported stimulation frequencies. When stable enough, this concept could extend to rapid-invisible stimulation, which operates above the critical flicker fusion frequency of perception (Seijdel, Marshall, & Drijvers, 2023). Even when using a low frequency of 3 Hz to drive the pulses, there may be deviations in pulse length or repeat gaps, making it uncertain whether the stimulation frequencies truly remained at 3 Hz. Ultimately, a way of validating pulse length needs to be implemented to ensure accuracy and reproducibility.

Conclusion

This pilot study has provided insights into the methodological and technical challenges associated with tracing ultrasound-based haptic neural markers. Moving forward, several key areas require focus to realize the full potential of employing SSEPs markers to ultrasound-based haptics. Firstly, future studies should prioritize the development of a fully synchronized setup between the EEG system and the ultrasound device, as time-locking the stimuli affords time-domain averaging of data. Additionally, strategies to mitigate effects of drowsiness and noise pollution, such as interactive tasks to maintain participant engagement and improved acoustic shielding, are strongly recommended. Furthermore, ensuring consistent stimulation frequencies and minimizing deviations of flicker pulses of the US array will enhance the reliability of SSSEP entrainment, leading to more robust and reproducible results.

The primary objective of this study was to pilot a method for establishing reliable neural markers for ultrasound-based haptics. I've found some evidence indicating successful SSSEP entrainment – these results however are quite noisy and underlie big variance between subjects and conditions. For stronger evidence, however, a refined experimental protocol with a bigger sample size is needed. This would make way for statistical analysis and generalizability of the findings.

This work paves the way for understanding the neural correlates of touchless haptic interfaces. As a next step, these markers will be compared against ones of conventional vibrotactile stimulation to assess their viability and provide a foundation for optimizing these interfaces for industry applications.

Bibliography

Abraira, V. E., & Ginty, D. D. (2013). The sensory neurons of touch. *Neuron*, 79(4), 618-639. https://doi.org/10.1016/j.neuron.2013.07.051

Alsuradi, H., Park, W., & Eid, M. (2020). EEG-based neurohaptics research: A literature review. *IEEE Access*, 8, 2979855. 10.1109/ACCESS.2020.2979855

ANTNeuro. (n.d.). $eego^{TM}$ mylab system with a 64-channel. ANTNeuro. Retrieved from https://www.ant-neuro.com/products/eego_mylab

Avanzini, P., Abdollahi, R. O., Sartori, I., Caruana, F., Pelliccia, V., Casaceli, G., Mai, R., Lo Russo, G., Rizzolatti, G., & Orban, G. A. (2016). Four-dimensional maps of the human somatosensory system. *Proceedings of the National Academy of Sciences*, 113(13), (pp. 1936-1943). https://doi.org/10.1073/pnas.1601889113

Breitwieser, C., Kaiser, V., Neuper, C., & Müller-Putz, G. R. (2012). Stability and distribution of steady-state somatosensory evoked potentials elicited by vibro-tactile stimulation. *Medical & biological engineering & computing*, 50(4), 347–357. doi: 10.1007/s11517-012-0877-9

Brickwedde M, Schmidt MD, Krüger MC, Dinse HR. 20 Hz Steady-State Response in Somatosensory Cortex During Induction of Tactile Perceptual Learning Through LTP-Like Sensory Stimulation. Front Hum Neurosci. 2020 Jun 30;14:257. doi: 10.3389/fnhum.2020.00257

Carter, T., Seah, S. A., Long, B., Drinkwater, B., & Subramanian, S. (2013). UltraHaptics: Multipoint mid-air haptic feedback for touch surfaces. In *Proceedings of the 26th Annual ACM Symposium on User Interface Software and Technology* (pp. 505–514). Association for Computing Machinery. https://doi.org/10.1145/2501988.2502018

Chouvardas, V. G., Miliou, A. N., & Hatalis, M. K. (2008). Tactile displays: Overview and recent advances. *Displays*, 29(3), 185-194. https://doi.org/10.1016/j.displa.2007.07.003

Cohen, M. X. (2022). A tutorial on generalized eigendecomposition for denoising, contrast enhancement, and dimension reduction in multichannel electrophysiology. *NeuroImage*, 118, 118809. https://doi.org/10.1016/j.neuroimage.2021.118809

Colon, E., Legrain, V., & Mouraux, A. (2012). Steady-state evoked potentials to study the processing of tactile and nociceptive somatosensory input in the human brain. *Journal of Neurophysiology*, 108(1), 316-327. doi: 10.1016/j.neucli.2012.05.005

Gramfort, A., Luessi, M., Larson, E., Engemann, D. A., Strohmeier, D., Brodbeck, C., Jas, M., Brooks, T., Parkkonen, L., & Hämäläinen, M. S. (2013). MEG and EEG data analysis with MNE-Python. Frontiers in Neuroscience, 7, 267. https://doi.org/10.3389/fnins.2013.00267

Harris, C. R., Millman, K. J., van der Walt, S. J., Gommers, R., Virtanen, P., Cournapeau, D., Wieser, E., Taylor, J., Berg, S., Smith, N. J., Kern, R., Picus, M., Hoyer, S., van Kerkwijk, M. H., Brett, M., Haldane, A., Fernández del Río, J., Wiebe, M., ... & Oliphant, T. E. (2020). Array programming with NumPy. *Nature*, 585(7825), 357-362. https://doi.org/10.1038/s41586-020-2649-2

Hoshi, T., Takahashi, M., Iwamoto, T., & Shinoda, H. (2010). Noncontact tactile display based on radiation pressure of airborne ultrasound. *IEEE Transactions on Haptics*, 3(3), 155-165. 10.1109/TOH.2010.4

Hoshi, T., Iwamoto, T., & Shinoda, H. (2009). Non-contact tactile sensation synthesized by ultrasound transducers. *In* 2009 World Haptics - Third Joint EuroHaptics Conference and Symposium on Haptic Interfaces for Virtual Environment and Teleoperator Systems (pp. 256-260). Salt Lake City, UT, USA. https://doi.org/10.1109/WHC.2009.4810848

imec. (2020, June). Haptic feedback: The next step in smart interfacing. *imec Magazine*. Retrieved August 1, 2024, from https://www.imec-int.com/en/imec-magazine/imec-magazine-june-2020/haptic-feedback-the-next-step-in-smart-interfacing

Large, D. R., Harrington, K., Burnett, G., & Georgiou, O. (2019). Feel the noise: Mid-air ultrasound haptics as a novel human-vehicle interaction paradigm. *Applied Ergonomics*, 81, 102874. 10.1016/j.apergo.2019.102909

Rosso, M. (2023). Human rhythmic interactions: Coordination dynamics and informational coupling (Doctoral dissertation, Ghent University, Belgium and University of Lille, France).

Seijdel, N., Marshall, T. R., & Drijvers, L. (2023). Rapid invisible frequency tagging (RIFT): A promising technique to study neural and cognitive processing using naturalistic paradigms. *Cerebral Cortex*, 33(5), 1626-1629. https://doi.org/10.1093/cercor/bhac160

Sénac, T., Lelevé, A., Moreau, R., Pham, M. T., & Novales, C. (2019). A review of pneumatic actuators used for the design of medical haptic training simulators. *Multimodal Technologies and Interaction*, 3(3), 47. https://doi.org/10.3390/mti3030047

Song, L., Glinsek, S., Uršič, H., Drnovšek, S., Šadl, M., Malič, B., & Defay, E. (2023). Power-efficient piezoelectric haptic actuators with large deflection. Sensors and Actuators A: Physical, 356, 114346. https://doi.org/10.1016/j.sna.2023.114346

Ultraleap. (n.d.). Ultraleap mid-air haptics. Ultraleap. Retrieved July 28, 2024, from https://docs.ultraleap.com/haptics/

Ultraleap. (2019). *Automotive UI study*. Retrieved June 12, 2024, from https://www.ultraleap.com/company/news/blog/automotive-ui-study/

Virtanen, P., Gommers, R., Oliphant, T. E., Haberland, M., Reddy, T., Cournapeau, D., Burovski, E., Peterson, P., Weckesser, W., Bright, J., van der Walt, S. J., Brett, M., Wilson, J., Millman, K. J., Mayorov, N., Nelson, A. R. J., Jones, E., Kern, R., ... & van der Walt, S. J. (2020). SciPy 1.0: Fundamental algorithms for scientific computing in Python. *Nature Methods*, 17(3), 261-272. https://doi.org/10.1038/s41592-019-0686-2

Vos, S., Collignon, O., & Boets, B. (2023). The Sound of Emotion: Pinpointing Emotional Voice Processing Via Frequency Tagging EEG. *Brain sciences*, 13(2), 162. 10.3390/brainsci13020162

Wen, H., & Liu, Z. (2016). Separating fractal and oscillatory components in the power spectrum of neurophysiological signal. *Brain Topography*, 29(1), 13–26. https://doi.org/10.1007/s10548-015-0448-0